International Journal of Biological Macromolecules 343 (2026) 150438

Contents lists available at ScienceDirect

International Journal of Biological Macromolecules

journal homepage: www.elsevier.com/locate/ijbiomac

Chestnut burrs as a sustainable source of cellulose for Pickering emulsion stabilisers

Joana Lains [a], Heloísa Almeida [b], Maria Filomena Barreiro [b], Cláudia Gomes Silva [a], Madalena M. Dias [a], Ricardo J. Santos [a], Andreia Ribeiro [a,*], Isabel M. Martins [a,*]

[a] LSRE-LCM, ALiCE, Faculty of Engineering, University of Porto, Rua Dr. Roberto Frias, 4200-465, Porto, Portugal
[b] CIMO, LA SusTEC, Instituto Politécnico de Bragança, Campus de Santa Apolónia, 5300-253, Bragança, Portugal

ARTICLE INFO

Keywords:
Chestnut burrs
Cellulose
Alkali hydrolysis
Bleaching treatment
Pickering emulsion

ABSTRACT

As the global population grows, increasing food consumption drives a significant rise in agri-food waste. In the northern Trás-os-Montes region of Portugal, one of the world's largest chestnut producers, this waste includes valuable by-products such as chestnut burrs, which are composed of 63% cellulose. This study aims to valorise chestnut burrs by extracting compounds for incorporation into high-added-value products. Cellulose was extracted through physical and chemical pre-treatments, alkali hydrolysis and bleaching. The process parameters were adjusted to enhance the extracted cellulose content and purity. Extracts were characterised by thermogravimetry and Fourier Transform Infrared Spectroscopy, and parameters such as particle size, zeta potential and wettability were also assessed and compared with commercial microcrystalline cellulose. Temperature was identified as the key parameter in alkali hydrolysis, with optimal conditions obtained for 10% NaOH at 100 °C for 1 h and a biomass-to-solvent ratio of 1:20 g/mL. Bleaching under optimal conditions (2% NaClO at 35 °C) removed an additional 7% lignin and enhanced the whiteness of the final product. The cellulose obtained has a purity of 72%, with a particle size of 55 μm, a negative surface charge, hydrophilic behaviour, an estimated molecular weight of 13.2 kDa, and a crystallinity of 56.5%. When applied at 0.8 *wt*% of the aqueous phase in 20:80 oil-in-water emulsions, these particles stabilise Pickering emulsions with a 12 mm average droplet size, remaining stable for at least 30 days. These findings demonstrate that chestnut burrs are a viable and sustainable source of cellulose with high potential as a natural Pickering emulsion stabiliser for use in food, cosmetics, and pharmaceuticals.

1. Introduction

Portugal is the 8th largest chestnut producer globally, harvesting around 24,000 t in 2022 [1]. The Trás-os-Montes region, located in the North of Portugal, accounts for approximately 85% of national production. The predominant species is *Castanea sativa Mill.*, also known as the European or sweet chestnut [2], and the harvest season occurs mainly in October [3]. This species belongs to *Fagaceae* family [2] and is widely used in various culinary applications such as marron glacé, purée, and chestnut flour, which are especially popular in gluten-free diets [4]. However, chestnut production generates solid waste, accounting for 15–20% of the total chestnut weight, primarily consisting of shells and burrs [5]. Shells are commonly used in biofuel production [6], and are also a potential source of polyphenols [6], while burrs — typically discarded — are notable for their high polysaccharide content, namely cellulose, as well as their antioxidant potential [5]. Additionally, chestnut cultivation generates substantial quantities of leaves, which are rich in bioactive compounds and have been used in traditional medicine for treating diarrhoea, infertility and cough [6]. Although the valorisation of chestnut flowers, leaves, and shells has been explored, the extraction of cellulose specifically from chestnut burrs remains unreported in the literature, revealing a clear gap that this study seeks to address.

Chestnut burr is a lignocellulosic husk forming the outer layer of chestnut fruit, rich in woody fibres and polyphenols. Its chemical composition comprises approximately 30% cellulose, 23% hemicellulose, 18% lignin, 14% total phenols [7], making it a competitive cellulose source compared with other residues such as pineapple crown (56%) [8], apple pomace (33%) [9], sugar palm (51%) [10], belulang grass (*Eleusine indica*) (34%) [11], cashew nut shell waste (18%) [12],

* Corresponding authors.
E-mail addresses: asribeiro@fe.up.pt (A. Ribeiro), isa@fe.up.pt (I.M. Martins).

https://doi.org/10.1016/j.ijbiomac.2026.150438
Received 30 September 2025; Received in revised form 19 January 2026; Accepted 20 January 2026
Available online 21 January 2026

pine sawdust (52%) and maize stalk (46%) [13].

Lignocellulosic materials are complex structures formed by fibrils of cellulose interconnected by hemicellulose and covered by lignin, making these materials very resistant and rigid [14]. Cellulose, the most abundant biopolymer on earth, is a linear homopolysaccharide composed of D-anhydroglucopyranose (AGU) units linked by b(1–4) glycosidic and hydrogen bonds [15]. Structurally, cellulose contains both highly crystalline ordered regions and amorphous regions with more disordered and branched chains [15]. This compound is a renewable resource found in plants, trees, shells, husks and seeds, and has attracted growing interest due to its environmental benefits and desirable properties—such as biocompatibility, nontoxicity, biodegradability, and strong mechanical performance—make it valuable across sectors including food, cosmetics, and pharmaceuticals. Looking ahead, the development of cellulose-based materials will focus on improving durability under harsh conditions, reducing production costs, and expanding applications in sustainable technologies [12,16].

Isolating cellulose from lignocellulosic materials requires a sequence of treatments, including physical or chemical pre-treatment, hydrolysis (alkali, acid, enzymatic, or combination [17,18]), and a bleaching step. Pre-treatment aims to increase the surface area, decrease the degree of polymerisation, and remove extractives and part of the hemicellulose [14]. During hydrolysis, hemicellulose and lignin are broken down by nucleophilic attacks, dissolving them in the reaction medium, while cellulose fibres remain insoluble [19]. Bleaching is then applied to remove residual lignin resistant to hydrolysis and confer a lighter colour to the final product [20]. The effectiveness of these treatments depends on various parameters, such as solution type and concentration, reaction time, temperature, pH, and biomass-solution ratio [9,20,21].

Among the hydrolysis treatments, alkali and acid hydrolysis are the most commonly used. Alkali hydrolysis saponifies ester bonds, breaking links between hemicellulose and lignin, while acid hydrolysis efficiently cleaves cellulose glycosidic bonds, often yielding nanoscale products [22]. Enzymatic hydrolysis, which uses enzymes to break specific bonds, is generally reserved for high-purity cellulose applications (e.g., pharmaceuticals) or glucose production (via cellulase), due to its high cost [23].

Emulsions are mixtures of immiscible liquids, where one liquid is dispersed within the other in the form of small droplets, typically forming either oil-in-water (O/W) or water-in-oil (W/O) systems [24]. Traditionally, emulsions are stabilised by amphiphilic molecules – surfactants - that adsorb at the oil-water interface. Pickering emulsions (PEs), an alternative to traditional emulsions, are stabilised by solid particles which form a physical barrier capable of stabilising the droplets and preventing coalescence [25]. The absence of surfactants, easy production, and enhanced stability have driven growing interest in the food, cosmetic, and pharmaceutical industries [26].

The solid particles used to stabilise PEs can be inorganic or organic. Inorganic particles include materials such as silica, calcium carbonate, and hydroxyapatite [25], while organic particles often comprise biopolymers like cellulose, starch, or chitosan [27]. Increasingly, attention has turned to using particles derived from agricultural by-products or industrial residues, such as microcrystalline cellulose from plant biomass [28] or protein-rich particles from food processing waste [29]. These bio-based particles offer functional stabilisation and align with circular economy principles, enhancing the sustainability profile of Pickering emulsions [27,29].

In this context, the present study hypothesises that cellulose extracted from chestnut burrs can function as an efficient, bio-based stabiliser for Pickering emulsions, offering a sustainable alternative for formulations in different applications. The extraction parameters were studied to improve the cellulose extraction efficiency. Emulsion stability was assessed over 30 days by physical and organoleptic analysis. Rich in monounsaturated fatty acids, polyphenols, and vitamins E and A, sweet almond oil was selected as the oil phase for its health-promoting properties and broad applicability across various fields [30].

Beyond cellulose extraction, this study demonstrates for the first time the potential of chestnut burr-derived cellulose to act as a natural stabilising agent in Pickering emulsions. Unlike most microcellulose-based Pickering stabilisers reported in the literature, which originate from well-established sources such as wood pulp or agricultural residues with long research histories, chestnut burrs remain an almost entirely unexplored biomass despite being generated in large quantities and typically discarded without valorisation. This work therefore introduces a previously untapped cellulose source and reveals its unexpectedly high emulsifying efficiency, even at low particle loadings. These findings open new possibilities for their application in sectors such as food, cosmetics, and pharmaceuticals, where environmentally friendly and biodegradable alternatives to synthetic emulsifiers are increasingly in demand. By valorising an underutilised agricultural by-product, this work contributes to advancing sustainability in the industry.

2. Materials and methods

2.1. Materials

The raw material, chestnut burrs, was provided by *Parque Natural de Montesinho*, located in Trás-os-Montes region (Portugal). The burrs were collected in October 2023, during the chestnut harvesting season.

Commercial microcrystalline cellulose powder (CAS NO. 9004-34-6) derived from cotton linters, used for comparison, was acquired from MP Biomedicals, LLC (Germany). Sodium hydroxide (NaOH) was supplied by LabKem (CAS NO. 1310-73-2), sodium hypochlorite 10% (NaClO) by Limpolar (CAS NO. 7681-52-9), and the hydrogen peroxide (H_2O_2) by VWR (CAS NO. 7722-84-1). Copper (II)-ethylenediamine complex (CED) at 1 M aqueous solution (CAS NO. 14552-35-3) was supplied by Acros Organics.

The oil phase, sweet almond oil (CAS NO. 8007-69-0), was purchased from SPD, S.A. (Portugal). Nile red (CAS NO. 7385-67-3) and Calcofluor-white (CAS NO. 18909-100mL-F) were supplied by Sigma Aldrich, and dimethyl sulfoxide (DMSO) by VWR Chemicals (CAS NO. 67-68-5).

Distilled water was further purified using a Milli-Q water purification system (TGI Pure Water Systems, Greenville, SC, USA).

2.2. Cellulose extraction

Cellulose extraction was carried out using a previously reported method [8] with some modifications. Chestnut burrs were first cut and milled using a ball mill (Retsch Mixer Mill MM200) operating at 25 s^{-1} for 15 min, achieving a particle size of around 85 μm. This equipment included two ceramic pots (10 mL), each loaded with two ZrO_2 balls.

The extraction process comprised hydrothermal pre-treatment, followed by alkaline hydrolysis and bleaching, all carried out using a thermocouple-equipped stirring plate. The hydrolysis treatment at temperatures above 100 °C was carried out in an autoclave (Uniclave 77) operating at 2 bar. For the hydrothermal pre-treatment, 10 g of milled chestnut burr powder was added to 250 mL of deionised water and stirred at 500 rpm and 70 °C for 4 h. The mixture was then filtered by vacuum with a paper filter (12–15 mm) to recover the solid fraction. This solid was submitted to alkali hydrolysis with sodium hydroxide at two concentrations (10 and 30%), under three temperatures (70, 100 and 120 °C) and reaction times of 1 and 2 h. Two biomass-to-alkali ratios, 1:10 and 1:20 g/mL, were evaluated.

After hydrolysis, the material was washed with deionised water until neutral pH, and then filtered and dried. The final bleaching step was carried out to study the effect of the bleaching agent (NaClO and H_2O_2), its concentration (2 and 4%), and temperature (35 and 70 °C), using a in a solid-to-liquid ratio of 1:40 g/mL under stirring (300 rpm) for 1 h. The resulting material was washed, filtered, dried, and milled (25 s^{-1}, 15 min).

2.3. Cellulose characterisation

The extracted cellulose was characterised using different analytical techniques, and its behaviour was compared with a commercial benchmark, microcrystalline cellulose. The chestnut burrs powder was also analysed to assess the changes that occurred during the extraction process.

2.3.1. Thermogravimetric analysis

Thermogravimetric (TG) analysis was conducted to assess the thermal stability and composition of the samples by monitoring mass loss as a function of temperature, allowing the identification and quantification of the lignocellulosic fractions based on their characteristic degradation temperatures. Approximately 10 mg of each sample (chestnut burrs, commercial cellulose and extracted cellulose) was placed in crucibles for analysis. Measurements were performed by heating the sample from 50 to 900 °C at a constant rate of 10 °C min^{-1} under air flow using a STA 490 PC/4/H Luxx Netzsch thermal instrument. The first derivative of TG graphs (dTG) represents the mass loss (% $°C^{-1}$), where well-defined peaks correspond to the main degradation temperatures.

2.3.2. Particle size

Particle size analysis was performed by light scattering (LS) using a Beckman Coulter LS23O (California, USA) coupled with Shortcut by LS software. This technique measures particle volume distribution for different sizes and determines the mean particle size, expressed as mean ± standard deviation (SD). For the analysis, commercial cellulose and extracted cellulose samples were dispersed in distilled water; measurements were carried out in triplicate to ensure reproducibility.

2.3.3. Zeta potential

Zeta potential (z) was measured to assess the stability of the aqueous suspensions and to provide information on the surface charge of the particles. Measurements were performed by electrophoresis using a Nano ZS90 Zetasizer instrument (Malvern Instruments Ltd.). Suspensions are generally considered stable when the absolute zeta potential exceeds 30 mV. For the analysis, the samples (commercial cellulose and extracted cellulose) were diluted in distilled water at a concentration of 0.1 *wt*%, with refractive index and absorbance values set at 1.504 and 0.01, respectively. Each measurement was carried out in triplicate, and the results are expressed as mean ± SD.

2.3.4. Wettability

Wettability was evaluated as an indicator of the hydrophobic or hydrophilic character of the particles. Contact angles below 90° indicate hydrophilic behaviour, while values above 90° indicate hydrophobicity. For this analysis, pellets (13 mm diameter and 1 mm thickness) of each sample (commercial cellulose and extracted cellulose) were prepared using a hydraulic press (PerkinElmer) at 10 tons for 2 min. The contact angle is measured using a Biolin Scientific – Theta Lite 100 (Dataphysics Instruments, Germany) equipment coupled with software based on the Laplace-Young equation. For each sample, the measurement is taken in triplicate with different pellets. Measurements were performed by placing approximately 6 μL of distilled water onto the pellet surface using a high-precision injector. The contact angle was recorded over 60 s, and the results are reported as mean ± SD.

2.3.5. Colour measurement

Colour measurements were performed using a CR-400 colourimeter (Konica Minolta, Japan), determining the L^* (lightness), a^* (redness) and b^* (yellowness) parameters. L^* represents luminosity (ranging from 0 for dark to 100 for light), a^* indicates the green-red component (−60 for green to 60 for red), and b^* corresponds to the blue-yellow component (−60 for blue to 60 for yellow). The colour was evaluated using the whiteness index (WI), calculated as:

$$\mathrm{WI}\ (\%) = 100 - \sqrt{(100 - L^*)^2 + a^{*2} + b^{*2}} \quad (1)$$

2.3.6. Confocal laser scanning microscopy

The morphology of the extracted solid particles was analysed by confocal laser scanning microscopy (CLSM). Cellulose suspensions are stained with a 0.1% (*v/v*) calcofluor-white solution (1 g L^{-1} in water). This analysis was carried out in a Leica TCS-SP5 AOBS (Leica Microsystems Inc., Heidelberg, Germany), and the images were processed using LasX software. Samples were mounted on slides, and the fluorescent dye was excited at a wavelength of 433 nm.

2.3.7. Scanning electron microscopy

Scanning Electron Microscopy (SEM) was used to confirm the particles' morphology and size. A small amount of sample was placed on a carbon adhesive support and analysed using a high-resolution desktop scanning electron microscope (Phenom ProX Desktop SEM) at 1000′ magnification.

2.3.8. Fourier transform infrared spectrometry

Fourier Transform Infrared Spectroscopy (FTIR) was used to identify the main structural components of the samples by detecting characteristic bands corresponding to specific bonds and molecular vibrations. The measurements were performed using a FTIR spectrometer (Nicolet 510-P, Thermo Fisher Scientific, USA) equipped with a MIRacle ™ Single Attenuated Total Reflectance ZnSe crystal plate accessory (PIKE Technologies, USA). Spectra were recorded in transmission mode over the range of 4000 to 600 cm^{-1}, at 4 cm^{-1} resolution and 128 scans per sample. A small amount of powder sample (chestnut burrs, commercial cellulose and extracted cellulose) was placed directly onto the crystal plate for analysis.

2.3.9. X-ray diffraction

X-ray diffraction (XRD) analysis was conducted in a PANalytical X'Pert Pro diffractometer equipped with an X'Celerator detector and a secondary monochromator. The analyses were performed at room temperature with a voltage of 40 kV and a current of 30 mA ($10° \leq 2\theta \leq 60°$; 0.017°/step; 100 s/step), and the data acquisition employed Bragg-Brandt geometry with Cu Kα radiation. The Segal equation (Eq. (2)) determines the Crystallinity Index (CrI),

$$CrI\ (\%) = \frac{I_{002} - I_{amorphous}}{I_{002}} \times 100 \quad (2)$$

where I_{002} refers to the maximum intensity of the crystalline peak (≈ 22°), and $I_{amorphous}$ is the intensity of the non-crystalline material (minimum in the 15–22° range).

2.3.10. Molecular weight determination

The CED solvent was previously diluted to 0.5 M with ultrapure water at a pH of 12 adjusted with 1% NaOH. The cellulose sample was completely dissolved in CED by continuous magnetic stirring at room temperature at a concentration of 0.06 g/mL. Then, samples at 0.01, 0.02, 0.03, 0.04, and 0.05 g/mL were prepared by diluting the 0.06 g/mL sample with 0.5 M CED solution. The viscosity was evaluated in units of mPa for the 6 concentrations using a rotary viscometer (series VR 3000, Myr) operating at 25 °C. It has been proven that the ratio derived from flow times measured by capillary viscosimeters equals the ratio between viscosities [31].

The viscosity average molecular weight, M_v, and degree of polymerisation, DP, were estimated by an empirical method that relates the increase in viscosity to the molecular weight of the polymer, according to the standard procedure [31]. Firstly, the relative viscosity, η_r, was calculated using the measured sample viscosities, η, and the viscosity of the 0.5 M CED solution, η_0, according to Eq. (3). The specific viscosity, η_{sp}, which represents the relative increase caused by the dissolved

polymer, was calculated using the relative viscosity, as expressed in Eq. (4). Then, Eq. (5) relates the specific viscosity with concentration to obtain the reduced viscosity, η_{red}. The inherent viscosity, η_{inh}, was calculated based on η_r, according to Eq. (6). The intrinsic viscosity, [η], was determined via Huggins' plot (i.e, the plot of η_{red} vs concentration) or Kraemer's plot (i.e., the plot of η_{inh} vs concentration, c) based on Eqs. (7) and (8), respectively. Then, the Mark-Houwink equation (Eq. (9)) relating the molecular weight of the polymer with the [η] at a specific temperature (25 °C), was used with constants K (0.029 $mL{\cdot}g^{-1}$) and a (0.80) obtained from the literature using the same experimental conditions (0.5 M CED solution at 25 °C and a molecular weight range of 20 to 120 kDa) [32]. Finally, the degree of polymerisation was obtained by Eq. (10).

$$\eta_r = \frac{\eta}{\eta_0} \tag{3}$$

$$\eta_{sp} = \frac{\eta - \eta_0}{\eta_0} = \eta_r - 1 \tag{4}$$

$$\eta_{red} = \frac{\eta_{sp}}{c} \tag{5}$$

$$\eta_{inh} = \frac{\ln \eta_r}{c} \tag{6}$$

$$[\eta] = \lim_{c \to 0} \frac{\eta_{red}}{c} \tag{7}$$

$$[\eta] = \lim_{c \to 0} \frac{\ln \eta_r}{c} \tag{8}$$

$$[\eta] = K \bullet M_w^a \tag{9}$$

$$DP = \frac{M_v}{162} \tag{10}$$

2.4. Pickering emulsion production

Pickering emulsions were produced in two steps following a previously described procedure [33]. First, the aqueous phase was prepared by dispersing cellulose particles in distilled water at concentrations ranging from 0.2 to 2.5 *wt%*. Ultrasound treatment was performed for 1 min at 25 s^{-1} amplitude to reduce the particle size and improve dispersion. The oil phase was gradually added to the prepared aqueous phase using a peristaltic pump set at 120 rpm, approximately 50 mL/min. Emulsification was then carried out with a rotor-stator homogeniser (Miccra RT D-9, Mülheim, Germany) at 16000 rpm. After the oil addition, the system was stirred for a further 4 min at room temperature. The O/W emulsions were prepared to a final volume of 200 mL and a fixed oil/water ratio of 20:80.

2.5. Pickering emulsion characterisation

The emulsions were characterised immediately after production and during one month of storage at room temperature (sampling at 2, 7, 15, 21, and 30 days). Morphology was evaluated using optical microscopy (OM) and confocal laser scanning microscopy (CLSM). Droplet size distributions were determined using light scattering, accompanied by visual inspection to check for instability phenomena.

2.5.1. Visual inspection

Emulsions were examined visually to check for instability occurrence (creaming, phase separation, or sedimentation), and the macroscopic appearance was registered using a photographic camera.

2.5.2. Optical microscopy

OM was used to assess droplet morphology and detect instabilities. This analysis was performed using a Carl Zeiss Axiotech 100 HD optical microscope (Zeiss Instruments, Jena, Germany), fitted with a digital camera (AxioCam 105 colour). A small amount of sample was placed on a microscope slide, gently dispersed, and covered with a coverslip. Image acquisition was done using Zen software at magnifications of 5, 10 and 20′.

2.5.3. Droplet size

LS was used to determine the droplet size distribution and to evaluate coalescence phenomena, which lead to an increase in droplet diameter. The analysis was performed using the previously described equipment.

2.5.4. Confocal laser scanning microscopy

CLSM was used to observe the stabilisation mechanisms in the PEs. This analysis was conducted as previously described in Section 2.3.6. Both phases of PE samples were stained with fluorescent dyes: Nile red (1 g L^{-1} in DMSO) for the oil phase (green fluorescent) and calcofluor-white (1 g L^{-1} in water) for the cellulose particles (blue fluorescent). The emulsion was stained with a dye-to-sample ratio of 1:10. Fluorescence excitation was carried out at 488 nm for Nile red and 433 nm for calcofluor-white.

3. Results and discussion

3.1. Cellulose extraction

This section presents the results of the cellulose extraction process from chestnut burrs. The chemical pre-treatment performed can successfully remove a total phenolic content of 51.75 mg gallic acid equivalent/g biomass according to the Folin Ciocalteu method. The composition and effectiveness of the extraction and bleaching treatments were evaluated through thermogravimetric analysis (TG). Holocellulose, which comprises the combined polysaccharide fraction of cellulose and hemicellulose, degrades between 240 and 370 °C; within this range, hemicellulose decomposes at lower temperatures, while amorphous and crystalline cellulose degrade at progressively higher temperatures [34]. In contrast, lignin, being more thermally stable, degrades at higher temperatures, typically between 370 and 480 °C [35].

3.1.1. Alkali hydrolysis

To obtain a final product with high cellulose content and low lignin levels, a parametric study was conducted by varying the hydrolysis conditions, namely NaOH concentration, temperature, reaction time, and biomass-to-alkali solution ratio.

The initial hydrolysis conditions were based on a previous work [8], 1:10 g/mL biomass-to-alkali ratio, 10% NaOH at 70 °C for 2 h under stirring (500 rpm). The cellulose and lignin contents estimated by thermogravimetric analysis are summarised in Table 1.

For lignin hydrolysis through nucleophilic attack by the hydroxide ions, two concentrations of NaOH were studied. The resulting materials

Table 1
Cellulose and lignin contents of the obtained samples under different hydrolysis conditions, estimated by thermogravimetric analysis.

NaOH Concentration / %	Ratio / g/mL	Temperature / °C	Reaction Time / h	Cellulose Content / %	Lignin Content / %
10	1:10	70	2	65	24
30	1:10	70	2	64	25
10	1:20	70	1	65	23
10	1:20	100	1	68	23
10	1:20	120	1	74	23
10	1:20	100	2	68	23
10	1:10	100	2	67	23

were analysed by TG. Fig. 1-A shows that using 10% or 30% of NaOH results in similar mass loss between 240 and 370 °C, leading to similar cellulose content. These results indicate that 10% of NaOH is sufficient for effective lignin hydrolysis and removal.

Since hydrolysis temperatures reported in the literature typically range between 60 and 120 °C [14], the effect of temperature was studied by considering 70, 100 and 120 °C. Fig. 1-B shows that higher temperatures lead to more significant mass loss within the temperature range of cellulose degradation, suggesting a significantly higher cellulose content in the final extract. However, the difference in cellulose content between 100 °C and 120 °C was minimal. Considering the reduced particle stability at 120 °C, as indicated by the less negative zeta potential (−21.6 mV at 100 °C versus −15.7 mV at 120 °C), along with the higher energy cost associated with the elevated temperature, increasing the temperature is not justified. Additionally, the overall yields were identical under both conditions (32%), and cellulose-based recovery was slightly higher at 100 °C (35% versus 34% at 120 °C), further supporting the selection of the lower temperature.

The effect of reaction time for this process was also studied. TG analysis (Fig. 1-C) shows that the thermograms obtained for 1 and 2 h overlap, indicating no significant difference between these reaction times. Similar results have been reported in the literature [9], where 30 min of alkali hydrolysis (9% NaOH at 70 °C) was sufficient to achieve an extract with 84.98% cellulose content from apple pomace. These findings suggest that most lignin removal occurs within the first hour, and prolonging the process beyond this point is unnecessary.

The biomass-to-alkali solution ratio was further evaluated. A 1:20 g/mL ratio has been commonly used in previous studies [36]. Accordingly, the effect of increasing the alkali volume to 200 mL (1:20 g/mL) was analysed (Fig. 1-D). Although the difference between 1:10 and 1:20 ratios was minimal, a slightly higher cellulose content was reached at 1:20 ratio, indicating a marginal improvement in hydrolysis efficiency. Given its broader application in the literature [11,37] and potential for improved consistency, the 1:20 g/mL ratio was selected for this study.

In summary, temperature significantly affects hydrolysis efficiency, whereas reaction time shows no impact beyond 1 h. A lower NaOH concentration (10%) is sufficient for lignin removal, and a higher biomass-to-alkali ratio offers minimal benefit, aligning with established literature practices. Therefore, the optimal conditions for achieving a high cellulose content are a biomass-to-alkali ratio of 1:20 g/mL, 10% NaOH concentration, processing at 100 °C, and stirring at 500 rpm for 1 h, resulting in a mass yield of 32%.

3.1.2. Bleaching

After hydrolysis, a bleaching treatment was applied to remove the brown colour imparted by the residual lignin resistant to the hydrolysis treatment. To evaluate the effectiveness of this treatment, two bleaching agents were investigated: NaClO and H_2O_2. For NaClO, the impact of temperature (35 °C and 70 °C) was studied. For H_2O_2, both concentration (2 and 4%) and pH (7 and 14) were analysed with the temperature fixed at 70 °C. Bleaching time was not evaluated, as previous studies reported that it has no significant effect on yield, whiteness index, or residual lignin [21]. Therefore, the bleaching process was considered complete when no further colour change was observed, which occurred after approximately 1 h.

Thermograms for all tested conditions are shown in Fig. 2, and the corresponding estimated cellulose and lignin contents are summarised in Table 2. Fig. 2-A shows the effect of temperature using NaClO as a bleaching agent. The first mass loss, corresponding to cellulose degradation (240 to 350 °C), is higher at 70 °C than at 35 °C, which means that a higher temperature leads to extracts with higher cellulose content. These curves shift to lower temperatures, suggesting that the amorphous component of cellulose has increased. The literature reports that reactive oxygen species, such as those generated from NaClO, promote an oxidative delignification, causing the conversion of highly ordered crystalline regions into less ordered domains, thereby reducing the thermal stability of cellulose [38]. The mechanism involves the oxidation of ethylenic and carbonyl groups in lignin [39], a reaction that is particularly favoured under alkaline conditions. The mass loss curve referring to the lignin degradation (370 to 480 °C) also shifted to a lower

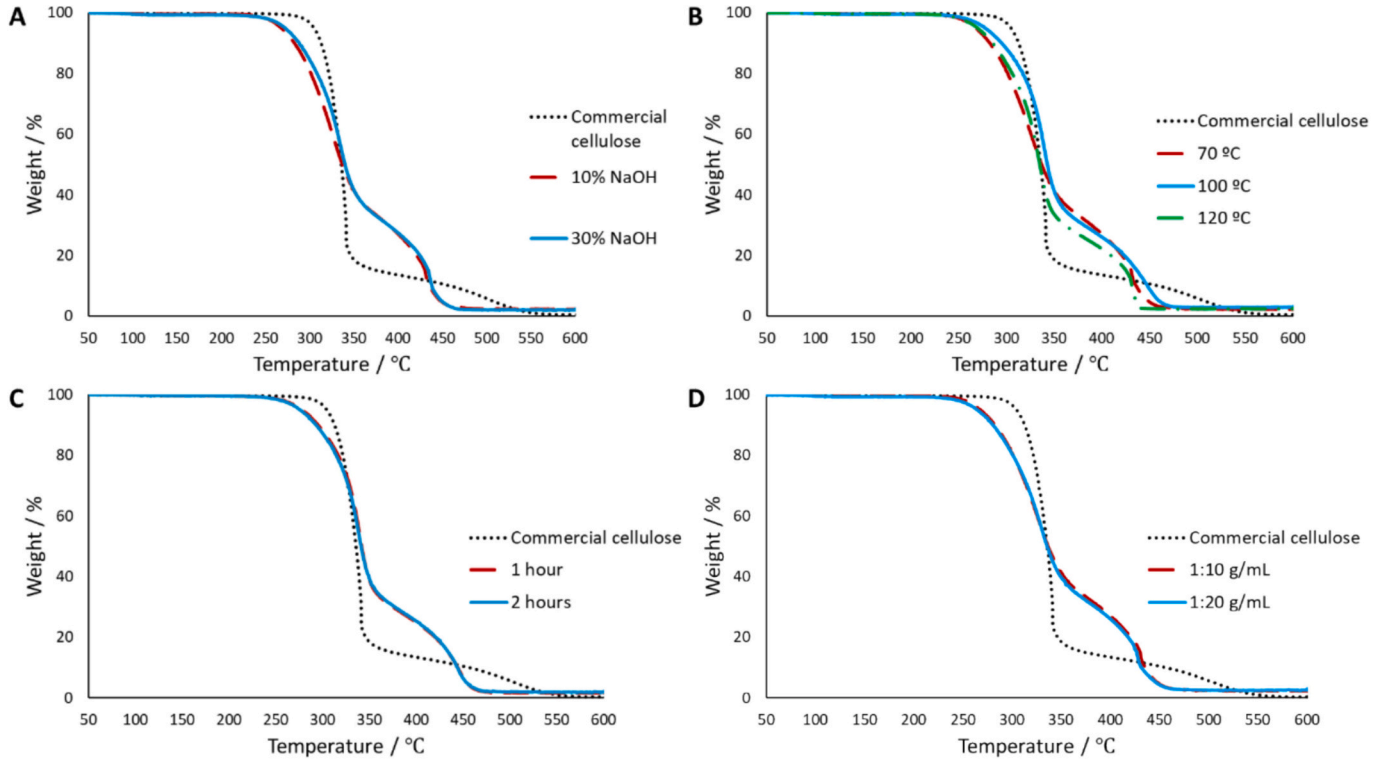

Fig. 1. Thermal degradation curves showing the effects of alkali solution concentration (A), temperature (B), reaction time (C) and biomass-to-alkali ratio (D) in the alkali hydrolysis.

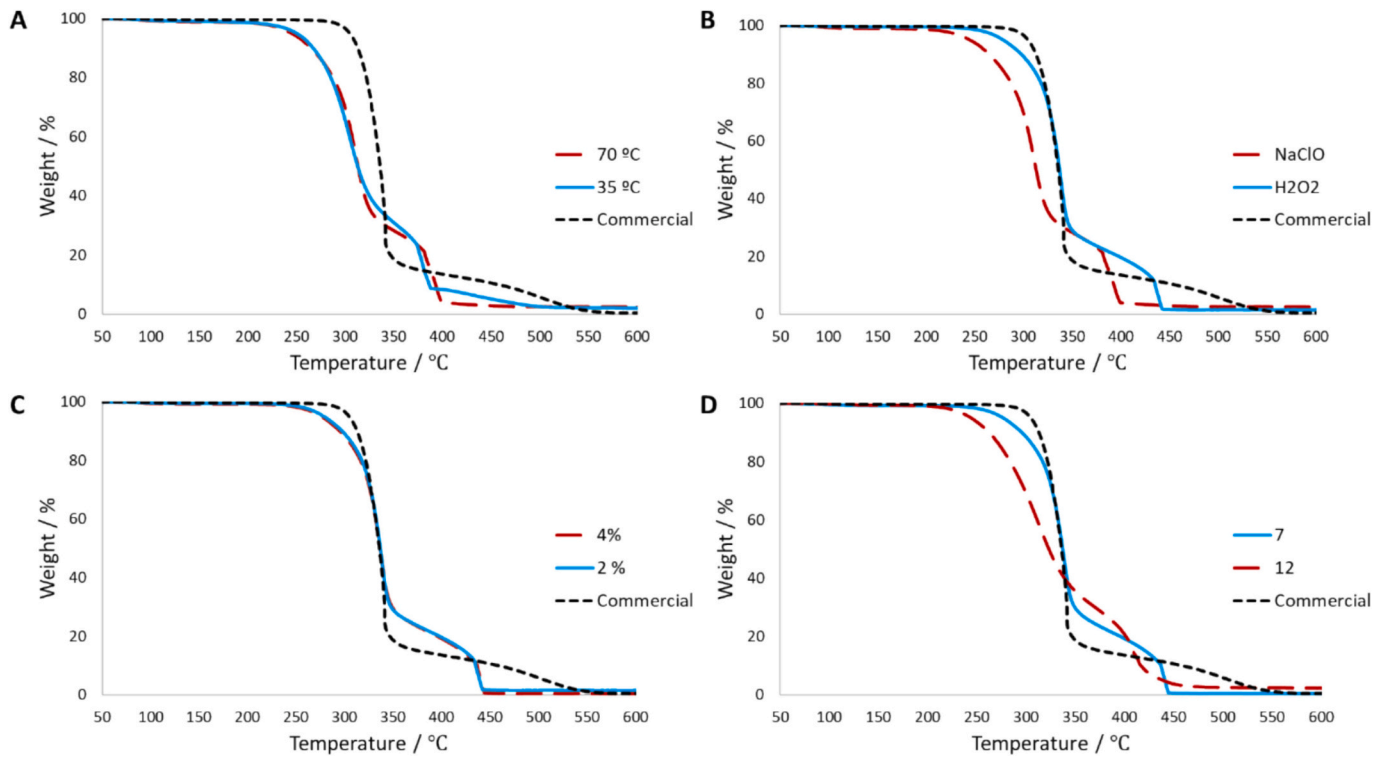

Fig. 2. Thermal degradation curves showing the effects of temperature (A), bleaching agent (B), H_2O_2 concentration (C) and pH using H_2O_2 (D) in the bleaching treatment.

Table 2
Estimated cellulose and lignin contents obtained by thermogravimetric analysis under different bleaching conditions.

Solvent	Concentration / %	Temperature / °C	pH	Cellulose Content / %	Lignin Content / %
NaClO	2	35	7	72	16
NaClO	2	70	7	74	21
H_2O_2	2	70	7	75	23
H_2O_2	4	70	7	75	24
H_2O_2	4	70	12	69	26

temperature since bleaching can convert lignin into a low-molecular-weight form [40]. In Fig. 2-B, which illustrates the effect of different bleaching agents, it is perceptible that these deviations are absent when the treatment is performed with H_2O_2 at neutral pH. This indicates that hydrogen peroxide helps preserve the crystalline structure. Analysis of Fig. 2-D (effect of pH in the H_2O_2 solution) shows this deviation again occurs at alkaline pH, confirming the previous conclusion.

Performing the treatments in a neutral medium with NaClO or H_2O_2 resulted in materials with similar cellulose content, but with different structures. When sodium hypochlorite is used, the degradation curves shift to lower temperatures, indicating an increase in amorphous cellulose content and enhanced solubilisation of lignin. In contrast, H_2O_2 under an alkaline environment result in lower cellulose content and higher lignin levels compared to a neutral environment.

Moreover, the TG analyses of the samples treated using different concentrations of H_2O_2 (Fig. 2-C) show similar degradation curves, indicating that increasing the concentration beyond 2% does not enhance the effectiveness of the bleaching treatment.

In summary, temperature is a key parameter, as its increase results in approximately a 2% rise in cellulose content. Additionally, the choice of bleaching agent affects both cellulose content and crystallinity. Cellulose bleached with H_2O_2 exhibits higher thermal stability, indicating a greater proportion of crystalline regions (or a reduction in amorphous regions). Finally, maintaining a neutral pH of the H_2O_2 solution is preferable, as no significant difference in cellulose content was observed when using an alkaline pH. Choosing the appropriate treatment parameters should take into account the intended product application, as these parameters affect not only the cellulose and lignin contents but also the material's structure, morphology, and properties.

To better evaluate the effectiveness of the bleaching step, the TG and respective derivative (dTG) curves of commercial cellulose, chestnut burr and the extracted cellulose before and after the bleaching treatment obtained with 2% NaClO, 35 °C, pH 7, are presented in Fig. 3. Commercial cellulose shows a well-defined peak at 341 °C in the dTG curve, indicating a predominantly crystalline cellulose structure, which confers greater thermal stability.

The first derivative of TG graphs (dTG) enhances the interpretation of TG data by highlighting the decomposition temperatures in well-defined peaks, aiding in the identification of sample components and their thermal behaviour. A peak observed around 300–350 °C typically corresponds to cellulose degradation, while the range of 370–480 °C is associated with lignin decomposition. Beyond this, the remaining material is primarily ash. Due to the greater thermal stability of crystalline regions, the higher the cellulose degradation, the greater the proportion of crystalline regions present in the sample.

Considering this information, by analysing the thermal profiles, it is observed that the chestnut burrs have hemicellulose, cellulose, lignin and other non-cellulosic compounds in their composition. Particularly, the chestnut burrs have a high content of cellulose, about 63%, according to the intensity of the corresponding peak.

The dTG curve of the extract obtained after hydrolysis shows two well-defined peaks: a first peak at 344 °C corresponding mainly to crystalline cellulose, and a second, less intense, peak at 451 °C associated with lignin degradation. These peak intensities suggest a composition of approximately 68% holocellulose and 23% lignin. After bleaching, the extract shows two major mass losses: the first at 309 °C, attributed to amorphous cellulose; and the second at 383 °C related to

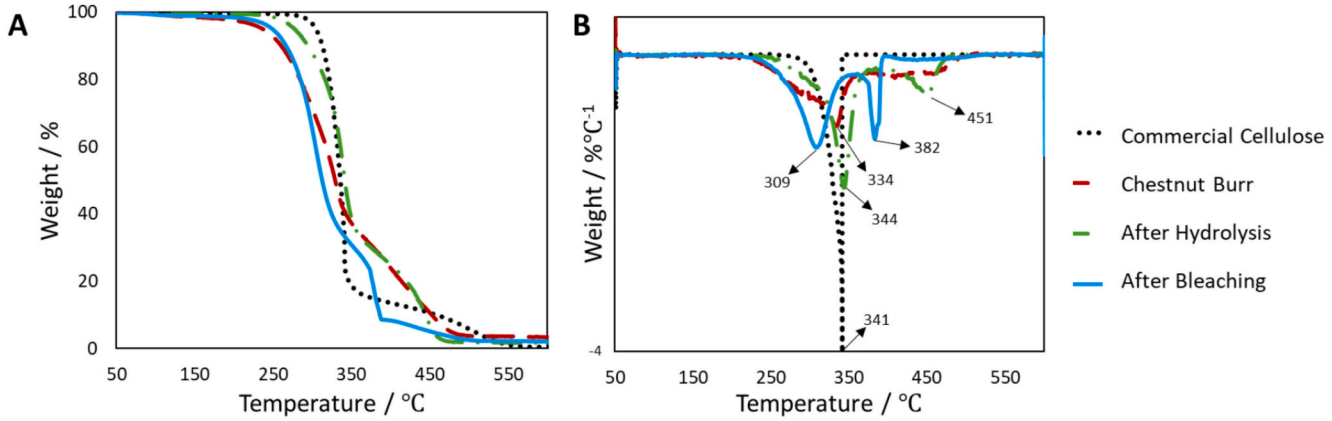

Fig. 3. Thermal degradation TG (A) and dTG (B) curves of commercial cellulose, chestnut burr, and extracted cellulose before and after bleaching.

more soluble lignin fractions. The bleached sample shows a 72% loss of mass associated with holocellulose, 16% to lignin, and the remaining 12% attributed to water and ash. This cellulose content is similar to values reported for pineapple leaf [11,41].

Overall, the bleaching process at 2% NaClO, 35 °C, pH 7 removes approximately 7% more lignin with a mass yield of 28% according to the initial biomass.

3.2. Cellulose characterisation

The materials obtained from the three bleaching conditions that led to higher cellulose contents (NaClO at 35 °C, NaClO at 70 °C, and 2% H_2O_2, all at 70 °C and under neutral pH) were characterised to assess the effect of the bleaching treatments on composition, stability, and colour properties.

3.2.1. Colloidal and surface properties

Table 3 shows the mean particle size determined by LS, the zeta potential, and the contact angle for the three selected materials, as well as for the commercial cellulose.

All the extracted cellulose particles are in the microscale range, varying between 50 and 80 mm, consistent with values reported for similar lignocellulosic materials [21,42], and comparable to the commercial cellulose.

The zeta potential of the material bleached with 2% H_2O_2 at 70 °C under neutral pH is relatively low (− 12.9 mV), indicating poor dispersion stability and a tendency for particle aggregation in aqueous media. This behaviour correlates with the higher contact angle observed, suggesting increased hydrophobicity and lower affinity for water. In contrast, the materials obtained after bleaching with NaClO exhibit zeta potential values close to - 30 mV, indicating greater stability in aqueous media. The zeta potential of the extract before bleaching was – 21.6 ± 1.35 mV, showing that bleaching NaClO treatment improves the stability of the aqueous suspensions.

The contact angle measurements further support these observations, as samples extracted with NaClO show lower contact angles compared to those obtained using H_2O_2. However, the extracted cellulose samples showed higher contact angle values compared to commercial cellulose, reflecting a reduced hydrophilicity. This behaviour is consistent with the presence of residual lignin and hemicellulose, as well as the lower crystallinity of the extracted fibres, which decreases surface polarity and limits the number of exposed hydroxyl groups. Therefore, the particles acquire a more amphiphilic character. This shift in wettability is particularly relevant for Pickering stabilisation, since particles that are too hydrophilic tend to remain in the aqueous phase and adsorb weakly at the oil–water interface, whereas particles with a moderately hydrophilic–amphiphilic nature fall within the optimal wettability window for O/W emulsions (between 60 and 80° [43]). The higher contact angle of the chestnut-burr cellulose increases the desorption energy, promoting stronger and more irreversible interfacial attachment.

Colour is a key quality parameter for cellulose, particularly its whiteness, which reflects the purity and degree of lignin removal. The whiteness index (*WI*) determined from lightness (*L**), redness (*a**) and yellowness (*b**) values was measured for commercial cellulose, chestnut burr, the extract after hydrolysis and extracted cellulose after bleaching (Table 4).

As expected, both chestnut burr and extracts obtained after hydrolysis show low WI values. Hydrolysis led to a 14% increase in WI, attributed to partial lignin removal. The bleaching treatment further improved whiteness, with WI increases ranging from 7% to 26% relative to the extract obtained after hydrolysis.

The high *WI* value of commercial cellulose (95.26%), a white powder, confirms its suitability as a reference material. Among the extracted cellulose samples, the highest WI was obtained after bleaching with 2% NaClO at 70 °C (86.14%), approaching that of commercial cellulose. In contrast, the lower value was obtained when H_2O_2 was used as the bleaching agent (67.42%).

3.2.2. Morphological analysis

Fig. 4 shows the CSLM images captured at 40× magnification, evidencing the morphology of the particles. The commercial cellulose presents an aggregation of cellulose fibres into cylindrical shapes with

Table 3
Particle size, zeta potential and contact angle for the three best bleaching conditions.

Bleaching conditions	Particle size / mm	Zeta potential / mV	Contact angle / °
Commercial microcrystalline cellulose	71.65 ± 0.79	-28.7 ± 0.35	34.03 ± 5.51
2% NaClO, 35 °C, pH 7	55.16 ± 0.47	-31.3 ± 0.76	57.58 ± 2.04
2% NaClO, 70 °C, pH 7	64.07 ± 2.01	-28.5 ± 1.04	50.11 ± 2.28
2% H_2O_2, 70 °C, pH 7	76.63 ± 1.66	-12.9 ± 0.87	63.83 ± 3.98

Table 4
Lightness (L*), redness (a*), yellowness (b*) values and the respective whiteness index (WI) for the commercial cellulose, chestnut burr and cellulose obtained after hydrolysis and after bleaching under different conditions.

Sample	*L**	*a**	*b**	*WI* / %
Chestnut burr	54.59	7.21	27.33	46.51
After hydrolysis	63.89	1.73	16.07	60.44
Commercial microcrystalline cellulose	96.83	−0.24	3.51	95.26
After bleaching at 2% NaClO, 35 °C, pH 7	89.77	−1.76	14.94	81.81
After bleaching at 2% NaClO, 70 °C, pH 7	90.16	−1.07	9.7	86.14
After bleaching at 2% H_2O_2, 70 °C, pH 7	74.81	0.63	20.65	67.42

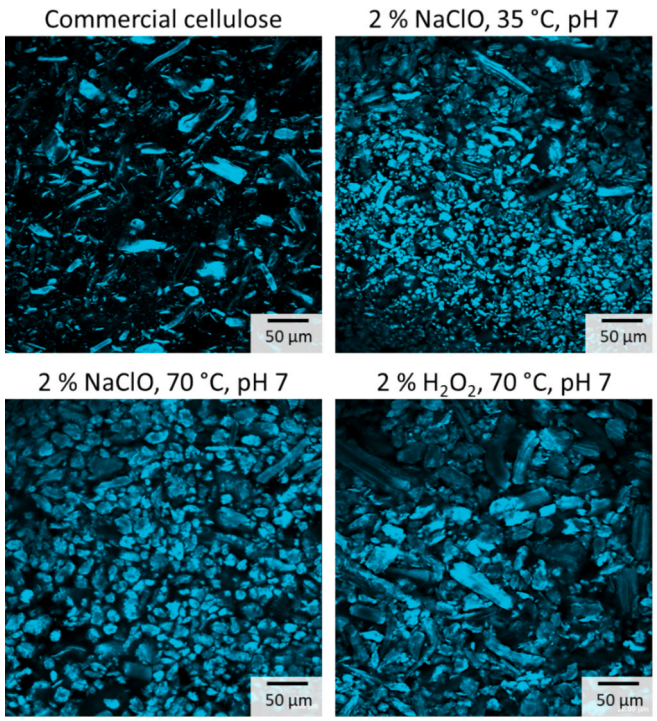

Fig. 4. CLSM images of commercial microcrystalline cellulose and extracted cellulose after bleaching. Magnification: 40 x.

varying particle sizes, which is expected due to its crystalline structure [44]. In contrast, particles obtained after NaClO bleaching show aggregation of the cellulose fibres in non-organised forms, leading to mostly spherical particles with a rough surface. Although some cylindrical and elongated particles are also observed, they are in smaller numbers. These observations confirm the conclusions drawn from the TG analysis, indicating a reduction in crystalline regions following NaClO bleaching. The shorter length and the different morphology of the particles suggest that NaClO causes structural damage to the cellulose fibres, possibly involving the breakdown of the b-1,4-glycosidic bonds, leading to fragmentation into smaller micro-cellulose particles. This behaviour has been previously reported and associated with excessive oxidation, causing irregular particles and size reduction [21,44]. The particles obtained after bleaching with H_2O_2 resemble commercial cellulose, displaying predominantly cylindrical and elongated shapes. This observation is consistent with the TG analysis, indicating the presence of numerous cellulose microcrystals along with some amorphous regions [44].

SEM analysis was performed to assess the structural changes to the raw material following the applied treatments. Representative micrographs are shown in Fig. 5, including the chestnut burrs powder, the hydrolysed extract and the final extracted cellulose obtained after bleaching with 2% NaClO at 35 °*C. SEM* image of the chestnut burr powder reveals a heterogeneous mixture of particles with varying sizes and morphologies. After alkali hydrolysis, the fibre structure appears more open, and the material exhibits increased homogeneity; however, the particles remain relatively dense and large. The subsequent bleaching treatment results in a noticeable increase in the number of smaller particles, suggesting the effective removal of surface impurities and further breakdown of larger particles into finer fragments. These morphological changes are consistent with findings from the previous CSLM analyses.

3.2.3. *Chemical structure*

The FTIR spectra of the materials obtained under different bleaching conditions are presented in Fig. A.1 (Supplementary Material). Fig. 6 shows the spectra of the chestnut burr powder, the extract obtained after hydrolysis, the extracted cellulose after bleaching with 2% NaClO at 35 °C, and the commercial cellulose. The main absorption bands, along with their corresponding bonds, vibrations, and associated components, are summarised in Table 5.

The chestnut burrs spectrum exhibits characteristic lignin adsorption bands at 1718 and 1603 cm^{-1}, along with the bands corresponding to cellulose at 1159, 1027 and 894 cm^{-1}, confirming the presence of both components in the raw material. Analysis of the spectra after alkali hydrolysis and after bleaching shows progressive attenuation of the lignin bands, indicating lignin removal throughout the extraction process. The similarities between the spectra of commercial cellulose and the bleached extracted cellulose, particularly in the intensity of the bands at 1159, 1027 and 894 cm^{-1}, confirm the successful extraction and high cellulose content of the final product [11,15,42,44]. Notably, the increasing intensity of the 1027 cm^{-1} band from chestnut burr to the hydrolysed extract, and further to the bleached extract, reflects the progressive increase in cellulose content and reduction of lignin. This band, attributed to the C – O stretching vibration between cellulose chains [44], reflects the linear and rigid molecular structure of cellulose. The peak at 894 cm^{-1} is assigned to the β(1 → 4) glycosidic bonds (–C1–O–C4–) characteristic of cellulose [36]. The stronger 3329 cm^{-1} peak observed for samples extracted with NaClO compared to those with H_2O_2 (Fig. A.1 – Supplementary Material) aligns with the wettability measurements, suggesting that NaClO treatment yields more hydrophilic cellulose [15]. Overall, the bleaching trials produced similar FTIR

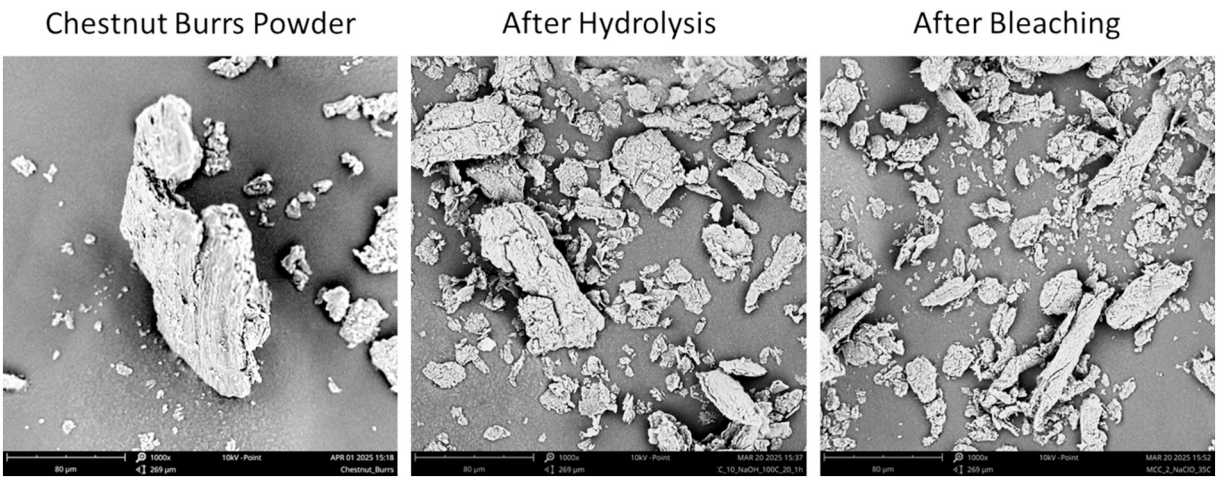

Fig. 5. SEM images of chestnut burrs, extract obtained after hydrolysis step and extracted cellulose after bleaching. Magnification: 1000×.

spectra, with consistent band positions but varying intensities depending on the remaining content of each component.

3.2.4. Crystallinity

X-ray diffraction (XRD) analyses were performed to infer about the crystallinity of the extracted samples. Diffractograms of commercial microcrystalline cellulose, and the resulting products after hydrolysis and bleaching performed with 2% NaClO and 2% H_2O_2 are presented in Fig. 7. The main peaks exhibited in all samples at 15.4°, 22.7° and 34.7°, corresponding to the 101, 002 and 040 crystallographic planes of cellulose type I, respectively [44]. This confirms that the process applied can successfully extract crystalline cellulose type I from chestnut burrs. The difference in intensity and peak width at 22° between commercial cellulose and our samples indicates that the resulting product has lower crystallinity and a larger crystal size. Moreover, the residual peak at 27° is attributed to the 101 lattice plane assigned to the reflection of crystalline silica (SiO_2) [45], indicating the presence of residual inorganic matter in the extracted material. This appearance indicates minor inorganic contamination, due to the accumulation of soil-derived minerals in the outer surface of chestnut burrs [46,47].

The CrI values calculated using Eq. (2) were 84.1%, 57.6%, 56.5% and 63.6% for commercial cellulose, the hydrolysed sample, the NaClO-bleached sample, and the H_2O_2-bleached sample, respectively. These results confirm that NaClO bleaching reduces crystallinity. The CrI values obtained are in agreement with biomass cellulose-derived reported in literature, such as 55% for melon residues [44] and 53% for fallen leaves [42]. However, they remain lower than those obtained from more crystalline sources, including cotton linter (75%) [48], sugarcane bagasse (77%) [15], and pineapple leaves (73%) [41].

3.2.5. Molecular properties

The molecular weight was estimated from intrinsic viscosity measurements using the Mark–Houwink equation, and both Huggins' and Kraemer's extrapolations were evaluated. Although the Huggins' plot yielded inconsistent and highly negative intercepts due to increased viscosity at higher concentrations, indicating deviation from ideal dilute-solution behaviour at the tested concentration range. This behaviour could be explained by aggregation or shear sensitivity [49–51]. Therefore, Kraemer's plot enables estimating a reasonable intrinsic viscosity using the linear region at dilute concentrations (0.01 to 0.04 $g{\cdot}mL^{-1}$) to minimise concentration-dependent effects, where the behaviour is closer to ideal. Based on Kraemer's intercept, the intrinsic viscosity of cellulose was 57.22 $mL{\cdot}g^{-1}$. This value suggests a molecular weight (M_v) of 1.32 × 10^4 $g{\cdot}mol^{-1}$, corresponding to a degree of polymerisation (DP) around 81. This value falls within the lower range typically reported for microcrystalline cellulose (MCC), which commonly exhibits DPs of 60 for cellulose with two chiral structures [52], or 130 for cellulose treated with 20% NaOH [53]. Thus, the cellulose extracted in this work shows a low DP, characteristic of microcrystalline cellulose, offering advantages such as non-toxic, low density and biodegradability [54]. Moreover, the M_v obtained is similar in magnitude, 10^4 $g{\cdot}mol^{-1}$, to values reported in the literature [52,53,55].

Table 5
Assignments of the absorption bands present in the FTIR spectra.

Wavenumber / cm^{-1}	Corresponding bonds	Associated component
3329	-OH stretching vibration	Cellulose/Lignin
2890	C-H stretching vibration	Cellulose/Lignin
1718	Acetyl groups and ester groups	Phenolic compounds linked to lignin
1603	Vibrations of aromatic rings	Lignin
1414	Flexing of CH_2	Cellulose
1313	CH deformation	Cellulose
1159	C-O stretching	Cellulose
1027	C-O-C asymmetrical stretching	Cellulose
894	β(1 → 4) glycosidic bonds	Cellulose

3.3. Pickering emulsion characterisation

Pickering emulsions were prepared using cellulose, with a purity of 72%, extracted from chestnut burrs under bleaching conditions of 2% NaClO at 35 °C and pH 7. The selection of these particles for PE production was based on their emulsifying performance, which is related to their structural and surface properties. The potential of a solid particle to properly stabilise a PE depends on its wettability, particle size, shape and stability [25]. Particle wettability determines the emulsion type and the particle/oil interactions; the size of solid particles must be smaller than the droplets formed, and the shape influences the interfacial coverage and network properties [25]. For the formation of stable Pickering emulsions, smaller particles exhibiting an absolute Zeta potential greater than 15 mV are preferred [25], since Zeta potential values between - 15 and 15 mV have been associated with particle aggregation and flocculation in suspension. Thus, the zeta potential was measured after ultrasound treatment, and the particles obtained with 2% NaClO at 35 °C presented the highest absolute value of 32.5 ± 0.43 mV.

Emulsions with a 20:80 O/W ratio were prepared using particle concentrations ranging from 0.2 and 2.5 *wt*% and characterised over one month of storage at room temperature (sampling time: 0, 2, 7, 15, 21 and 30 days). Fig. 8 shows the macroscopic appearance (vial photographs) and OM images for the emulsions at different concentrations and

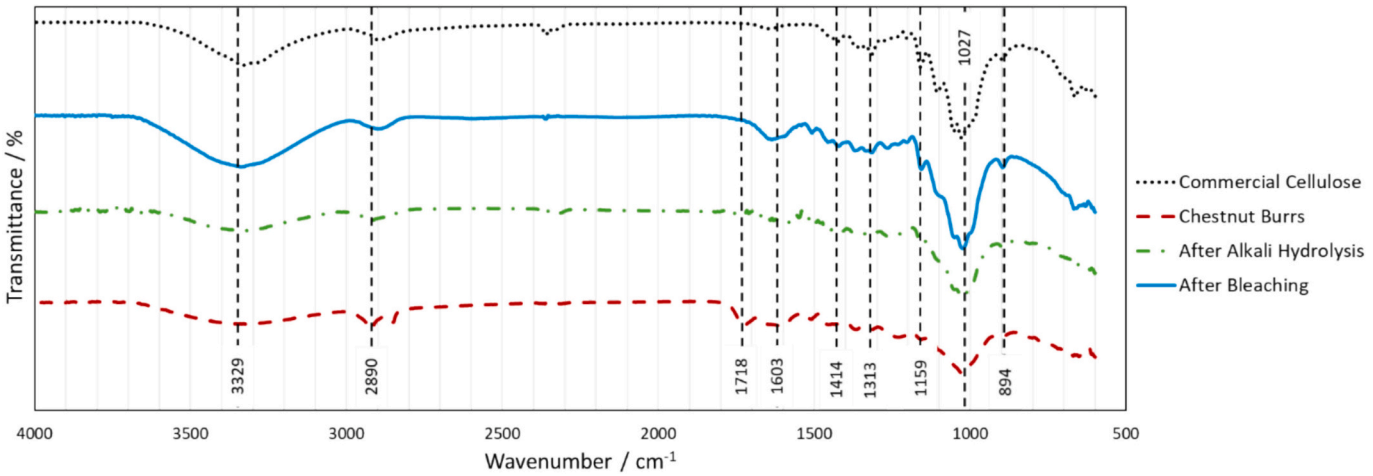

Fig. 6. FTIR spectra of commercial cellulose, chestnut burr, extract after hydrolysis and extracted cellulose after bleaching.

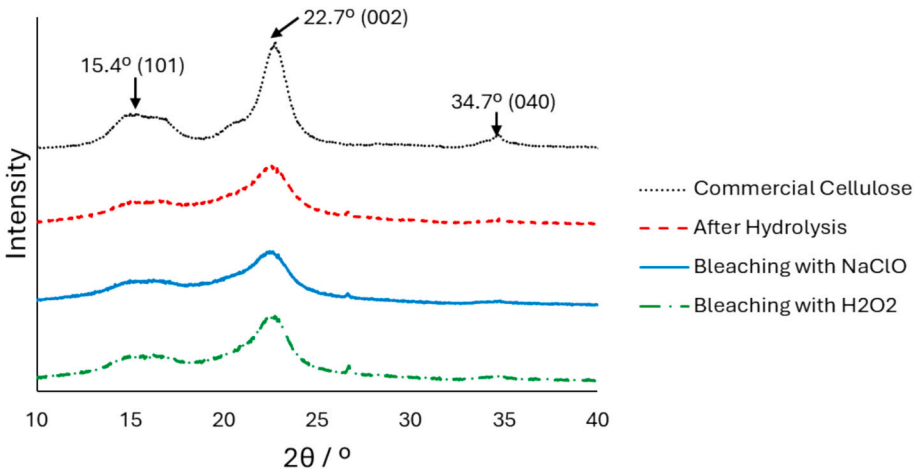

Fig. 7. XRD diffractograms of commercial cellulose, extract after hydrolysis, and cellulose obtained by NaClO-bleached and H_2O_2-bleached.

selected storage times (0, 15 and 30 days).

All emulsions exhibit some sedimentation shortly after production, which may be attributed to the high density of cellulose particles. Although the contact angle is below 90°, indicating an overall hydrophilic character, the value of approximately 60° suggests that the particles still possess a certain degree of affinity for the oil phase, which can contribute to sedimentation. Nevertheless, all droplets formed immediately after production presented a spherical shape.

At the lowest concentration (0.2 *wt*%), free oil is visible at the surface immediately after production and increases during storage. After 2 days, OM images show non-spherical droplets with a significant size variation. A creaming phase developed after 7 days and remained throughout the storage period.

At 0.5 *wt*%, the instability occurred later, with free oil detected at 15 days. Through the OM image, at 15 days, the coalescence of the droplets can be observed, and a creaming phase appears after 15 days of storage.

The higher concentration (2.5 *wt*%), oil droplets were stable for up to 15 days, but significant sedimentation of excess particles was observed. After this period, a creaming phase and some free oil appeared. At 1.5 *wt* %, sedimentation also occurred, but creaming developed earlier compared to 2.5 *wt*%.

The most stable emulsion was observed for 0.8 *wt*%, where droplets maintained their shape and size over the entire storage period. Visually, the emulsions appeared homogeneous after a slight agitation. This concentration appears sufficient to stabilise PEs using the extracted cellulose particles. Similar critical concentrations for cellulose-based PEs have been previously reported. For 20:80 O/W PEs, 0.8 *wt*% was found to prevent phase separation over short storage times, though some separation appeared with prolonged storage [56]. At different O/W ratios, stability was achieved at 0.5 *wt*% for 30:70 emulsions [57] and between 0.75 and 2 *wt*% for 10:90 emulsions [58]. However, using a commercial microcrystalline cellulose, with 84% of purity, the required concentration increases to 7.5 wt% for the same O/W ratio, exhibiting stability up to 60 days [28].

Mean droplet size measurements over the storage period of one month are summarised in Table 6. For the 0.5 *wt*% emulsion, the mean droplet size increased significantly, indicating coalescence and loss of stability. For the 0.2, 1.5, and 2.5 *wt*% emulsions, the observed reduction in droplet size over time may be attributed to a high polydispersity of these systems. Since instability phenomena such as phase separation and creaming formation were identified, the emulsion tends to separate during sampling. As only a subset of droplets is sampled, the analysed population may not accurately reflect the full emulsion, potentially leading to an underestimation of the average droplet size. Consequently, creaming and sedimentation processes alter the distribution of droplets available for imaging or laser diffraction, an effect that is particularly pronounced at low particle concentrations. The 0.8 *wt*% emulsion maintained a consistent droplet size throughout the analysis, confirming its superior stability.

Moreover, the differences observed in droplet size across the concentrations evaluated can be rationalised as follows: at low particle concentrations, insufficient interfacial coverage leads to partial coalescence and free-oil release, leaving a dispersed phase enriched in smaller droplets; at intermediate concentrations, increased particle availability enhances interfacial saturation during homogenisation, yielding smaller droplets; at high concentrations, the excess non-adsorbed particles form a three-dimensional network surrounding the droplets and producing an apparent increase in the measured droplet size.

The mechanism of stabilisation was analysed by CLSM. Fig. 9 shows the oil droplets (stained green), the cellulose particles (stained blue), and the corresponding overlapped images, highlighting the interactions between the particles and the oil phase. The images suggest that stabilisation occurs primarily through the formation of a three-dimensional network of interconnected larger, elongated cellulose particles, which entrap oil droplets and prevent coalescence. In addition, smaller cellulose particles are observed adsorbed at the oil-water interface, reducing interfacial tension.

This dual stabilisation mechanism has been previously described [59], where network formation increased with particle concentration. Similar observations were reported, where both adsorption of smaller particles onto the oil surface and particle-particle interactions between larger particles leading to a three-dimensional network were observed [60,61]. In addition, it has been suggested that the adsorption of smaller cellulose particles occurs through depletion attraction, while the formation of the network structure is driven by steric hindrance [56].

The higher amorphous content of chestnut burrs-derived cellulose makes the particles less rigid, enhances their wettability, and allows partial deformation and rearrangement at the oil–water interface, compared to rigid, highly crystalline cellulose. This structural flexibility promotes efficient interfacial adsorption and formation of a particle network, even at low concentrations. In contrast, highly crystalline cellulose is mechanically rigid and less capable of interfacial rearrangement, resulting in poorer coverage and requiring substantially higher particle loadings to establish comparable network connectivity and stabilisation.

In a previous study from our group, a Pickering emulsion stabilised with 7.5 wt% commercial microcrystalline cellulose exhibited stability for up to 60 days [28]. The emulsion prepared in the present work using only 0.8 wt% chestnut burrs–derived cellulose achieved comparable stability, despite a ten-fold lower particle concentration and the same O/W ratio. This pronounced difference indicates that material origin, supramolecular organisation, and surface properties play a critical role in

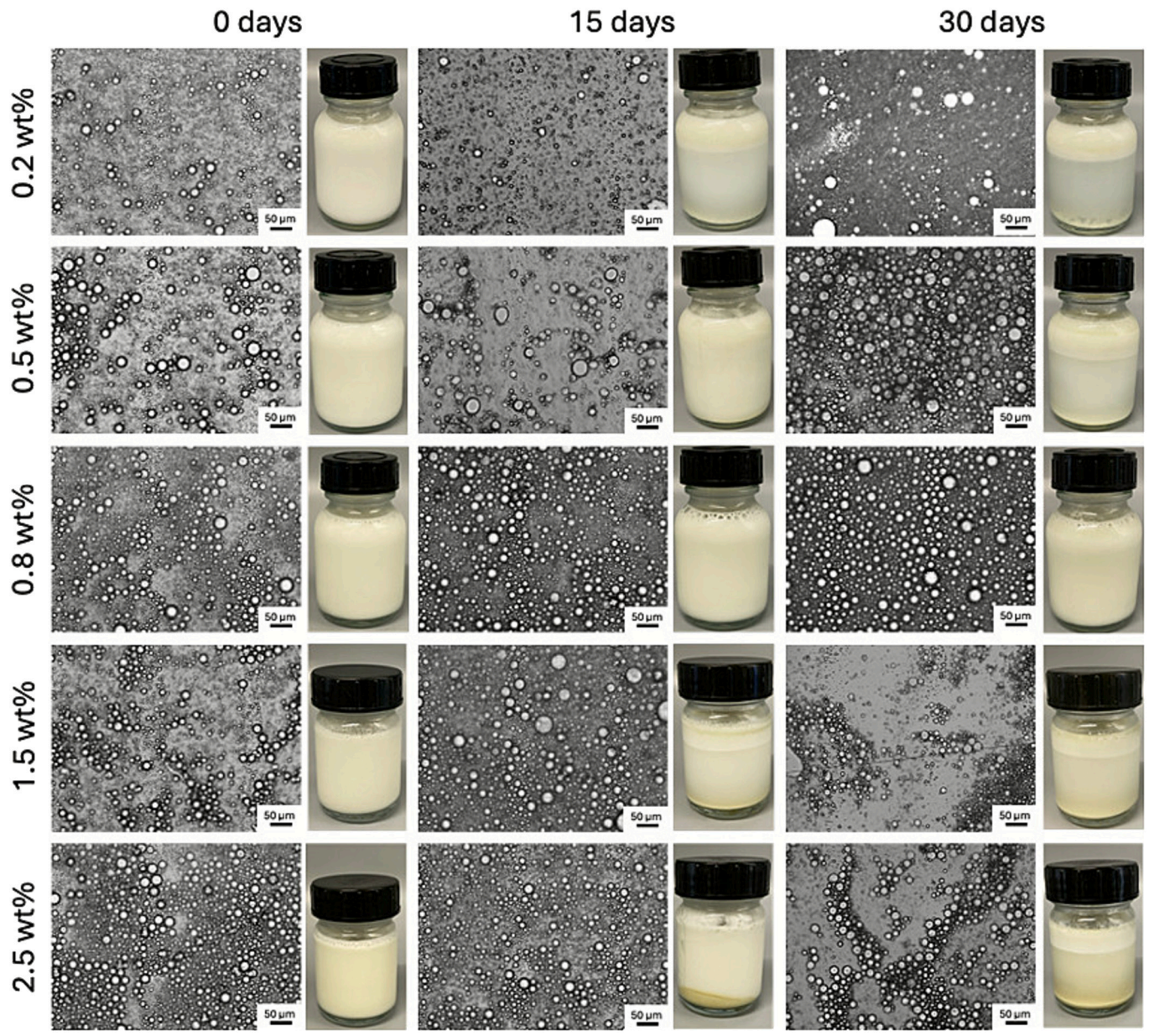

Fig. 8. Emulsion vial photographs and OM images of PEs showing the effect of cellulose particle concentration and storage time. All OM images were captured at 20 x magnification.

Table 6
Mean droplet size of PEs prepared with cellulose particles extracted from chestnut burrs over 30 days storage.

	Mean Droplet Size / mm		
Emulsion	0 days	15 days	30 days
0.2 *wt*%	8.93 ± 1.25	8.53 ± 0.96	6.71 ± 0.12
0.5 *wt*%	13.31 ± 0.50	13.52 ± 0.13	18.83 ± 0.85
0.8 *wt*%	12.39 ± 0.19	11.76 ± 0.22	14.76 ± 0.42
1.5 *wt*%	10.20 ± 0.42	12.53 ± 0.13	7.66 ± 0.38
2.5 *wt*%	13.08 ± 0.88	10.59 ± 0.37	8.16 ± 0.07

emulsifying performance. In the case of chestnut burr–derived cellulose, a dual stabilisation mechanism is observed: both the formation of a three-dimensional particle network and the adsorption of smaller cellulose particles at the oil–water interface contribute to droplet stabilisation. By contrast, commercial microcrystalline cellulose, being highly crystalline and rigid, stabilises emulsions primarily through network formation, with limited interfacial adsorption, requiring higher particle loadings. Consequently, emulsions stabilised with chestnut burr cellulose exhibited smaller and more uniform droplets (≈12 µm) compared with the larger droplets (≈18.7 µm) formed with microcrystalline cellulose, reflecting the enhanced interfacial activity afforded by its more amorphous and deformable structure. Overall, these results demonstrate the high efficiency of chestnut burr–derived cellulose as a natural, low-load Pickering stabiliser and highlight the functional advantages conferred by its amorphous character.

4. Conclusions

This study demonstrates the effective extraction of cellulose from chestnut burrs, an abundant and underutilised agricultural by-product. The extraction process involved sequential physical and chemical pre-treatments, followed by alkali hydrolysis and bleaching. Among the tested parameters, temperature was identified as the most influential variable in alkali hydrolysis, whereas reaction time had minimal impact

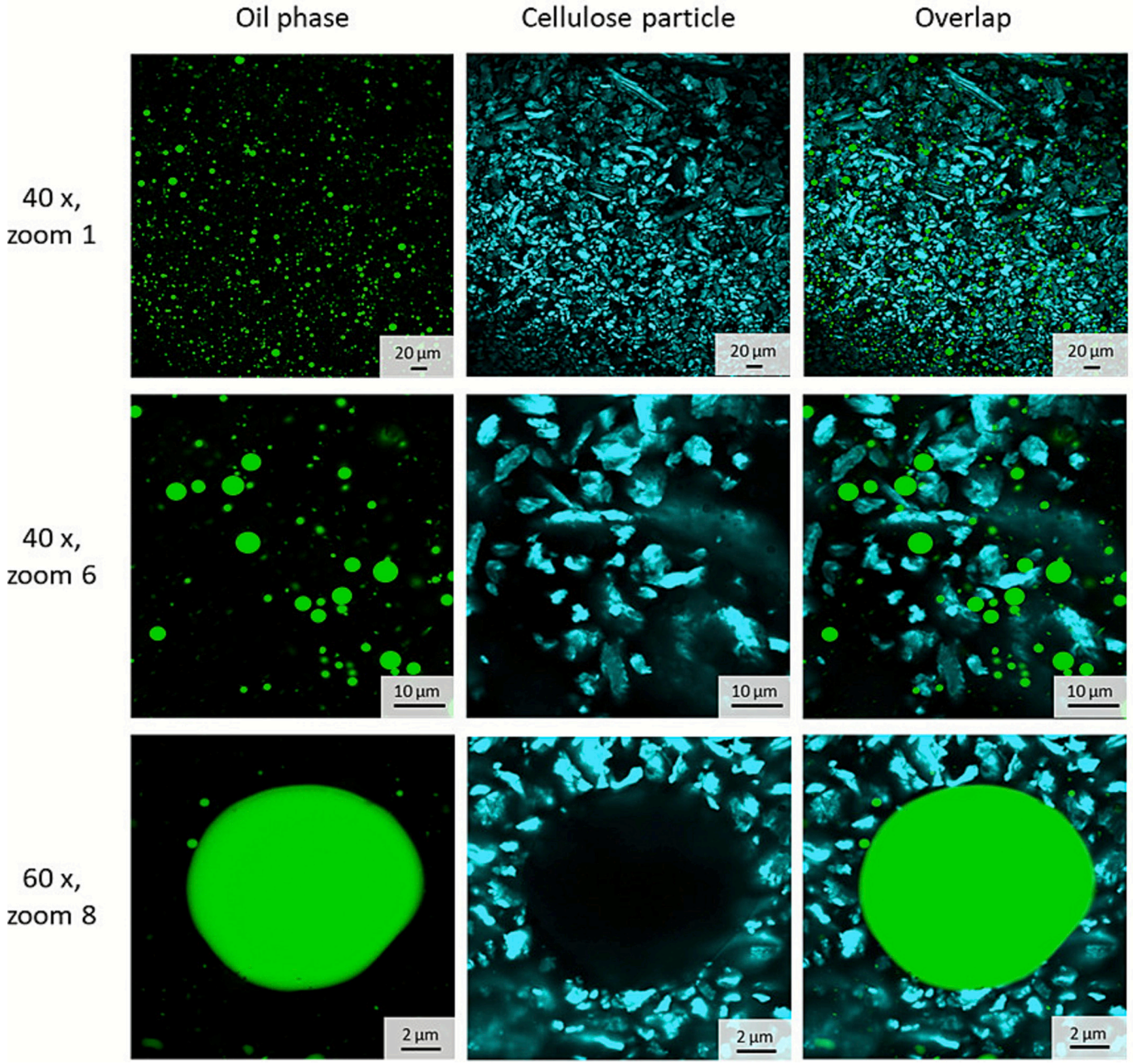

Fig. 9. CLSM images of 1.5 wt% PEs after 1 day storage time: oil phase in green (Nile red stain); cellulose particles in blue (calcofluor white stain). Images were registered at 40× magnification without zoom and at zoom 6, and 60× magnification with zoom 8.

beyond one hour. A 10% NaOH solution at 100 °C for 1 h and a biomass-to-solvent ratio of 1:20 g/mL yielded a cellulose-rich material with a content of 68% and a mass recovery of 32% from the initial biomass. Subsequent bleaching using 2% NaClO at 35 °C under neutral pH further improved the cellulose content to 72%, reduced lignin by an additional 7%, enhanced product whiteness, and decreased the mass yield to 28%. Given that the material is biomass-derived, a cellulose purity of 72% is relatively high and underscores the suitability of chestnut burrs as a promising cellulose source. Nevertheless, the remaining lignin and hemicellulose influence the physical properties of the material, so it must be carefully evaluated to ensure its suitability for the intended application.

The choice of bleaching agent used influenced the morphology of the cellulose particles. Sodium hypochlorite promoted the formation of more amorphous structures, whereas hydrogen peroxide preserved their crystalline component. When H_2O_2 is used, a concentration as low as 2% is sufficient, as higher concentrations do not lead to further improvement. Moreover, maintaining a neutral pH was essential to avoid structural degradation.

The resulting microparticles (~55 µm) displayed negative surface charge and hydrophilic behaviour, suitable for stabilising oil-in-water Pickering emulsions. At a concentration of 0.8 *wt*%, the extracted cellulose formed stable emulsions with droplet sizes around 12 µm, maintaining physical stability for at least 30 days. Confocal microscopy revealed that emulsion stabilisation occurred through a dual mechanism: particle adsorption at the oil–water interface and network formation that restricted droplet coalescence.

These findings highlight the potential of chestnut burr-derived microcellulose as an effective, biodegradable alternative to conventional surfactants. This approach contributes to the sustainable valorisation of agricultural residues and supports the development of natural emulsifiers for food, cosmetic, and pharmaceutical applications.

CRediT authorship contribution statement

Joana Lains: Writing – original draft, Validation, Methodology, Investigation. **Heloísa Almeida:** Investigation. **Maria Filomena Barreiro:** Writing – review & editing, Conceptualization. **Cláudia Gomes Silva:** Writing – review & editing, Methodology, Conceptualization. **Madalena M. Dias:** Writing – review & editing, Conceptualization. **Ricardo J. Santos:** Writing – review & editing, Conceptualization. **Andreia Ribeiro:** Writing – review & editing, Supervision, Methodology. **Isabel M. Martins:** Writing – review & editing, Supervision, Conceptualization.

Declaration of competing interest

The authors declare that they have no known competing financial interests or personal relationships that could have appeared to influence the work reported in this paper.

Acknowledgements

This work is financially supported by the Promove Programme through Fundação "La Caixa", in collaboration with the BPI and Fundação para a Ciência e a Tecnologia (FCT), under the project CyChest - Gestão integrada do ciclo do castanheiro no Parque Natural de Montesinho. This work was also financially supported by Fundação para a Ciência e a Tecnologia, I.P. /MCTES through national funds: LSRE-LCM, UID/50020/2025; and ALiCE, LA/P/0045/2020 (DOI: 10.54499/LA/P/0045/2020); CIMO, UIDB/00690/2020 (DOI: 10.54499/UIDB/00690/2020) and UIDP/00690/2020 (DOI: 10.54499/UIDP/00690/2020) and LA SusTEC, LA/P/0007/2021 (DOI:10.54499/LA/P/0007/2020). Andreia Ribeiro acknowledges the FCT for their research contract through the individual CEEC – Stimulus of Scientific Employment (DOI: 10.54499/2022.00798.CEECIND/CP1733/CT0009).

Appendix A. Supplementary data

Supplementary data to this article can be found online at https://doi.org/10.1016/j.ijbiomac.2026.150438.

Data availability

Data will be made available on request.

References

[1] Food and Agriculture Organization of the United Nations, Top 10 Country Production of Chestnuts, in Shell, 2024. https://www.fao.org/faostat/en/#rankings/countries_by_commodity. (Accessed 27 May 2024).
[2] D. Pinto, N. Braga, F. Rodrigues, M.B.P. Oliveira, Castanea sativa bur: an undervalued by-product but a promising cosmetic ingredient, Cosmetics 4 (2017) 50, https://doi.org/10.3390/cosmetics4040050.
[3] J. Gomes-Laranjo, L.-T. Dinis, L. Martins, E. Portela, T. Pinto, M. Ciordia, I. Feito, J. Majada, F. Peixoto, S. Pereira, Characterization of chestnut behavior with photosynthetic traits, Appl. Photosynth. 3 (2012) 47–80, https://doi.org/10.5772/26227.
[4] G. Squillaci, F. Apone, L.M. Sena, A. Carola, A. Tito, M. Bimonte, A. De Lucia, G. Colucci, F. La Cara, A. Morana, Chestnut (Castanea sativa Mill.) industrial wastes as a valued bioresource for the production of active ingredients, Process Biochem. 64 (2018) 228–236, https://doi.org/10.1016/j.procbio.2017.09.017.
[5] F.M. Vella, B. Laratta, F. La Cara, A. Morana, Recovery of bioactive molecules from chestnut (Castanea sativa Mill.) by-products through extraction by different solvents, Nat. Prod. Res. 32 (2018) 1022–1032, https://doi.org/10.1080/14786419.2017.1378199.
[6] D. Pinto, M. de la Luz Cádiz-Gurrea, A. Vallverdú-Queralt, C. Delerue-Matos, F. Rodrigues, Castanea sativa shells: a review on phytochemical composition, bioactivity and waste management approaches for industrial valorization, Food Res. Int. 144 (2021) 110364, https://doi.org/10.1016/j.foodres.2021.110364.
[7] J. Liang, J. Wu, J. Xu, Low-formaldehyde emission composite particleboard manufactured from waste chestnut bur, J. Wood Sci. 67 (2021) 1–10, https://doi.org/10.1186/s10086-021-01955-x.
[8] D. Choquecahua Mamani, K.S. Otero Nole, E.E. Chaparro Montoya, D.A. Mayta Huiza, R.Y. Pastrana Alta, H. Aguilar Vitorino, Minimizing organic waste generated by pineapple crown: a simple process to obtain cellulose for the preparation of recyclable containers, Recycling 5 (2020) 24, https://doi.org/10.3390/recycling5040024.
[9] A.Y. Melikoğlu, S.E. Bilek, S. Cesur, Optimum alkaline treatment parameters for the extraction of cellulose and production of cellulose nanocrystals from apple pomace, Carbohydr. Polym. 215 (2019) 330–337, https://doi.org/10.1016/j.carbpol.2019.03.103.
[10] N. Fitriana, A. Suwanto, T. Jatmiko, S. Mursiti, D. Prasetyo, Cellulose extraction from sugar palm (Arenga pinnata) fibre by alkaline and peroxide treatments, IOP Conf. Ser. Earth Environ. Sci. (2020), https://doi.org/10.1088/1755-1315/462/1/012053.
[11] A.W. Pratama, M. Mahardika, N. Widiastuti, B. Piluharto, R. Ilyas, S. Sapuan, D. Amelia, A. Firmanda, Isolation and characterization of highly thermal stable microcrystalline cellulose derived from belulang grass (Eleusine indica), Case Stud. Chem. Environ. Eng. 9 (2024) 100743, https://doi.org/10.1016/j.cscee.2024.100743.
[12] M. Palaniappan, S. Palanisamy, S. Tadepalli, N. Ayrilmis, T.M. Murugesan, Extraction and characterization of cellulose from Anacardium occidentale shells: a sustainable approach to industrial waste management, Int. J. Biol. Macromol. 320 (2025) 146120, https://doi.org/10.1016/j.ijbiomac.2025.146120.
[13] E. Makhado, W.M. Seleka, L. Mahlaule Glory, K. Selowa, M.H. Abu Elella, O. J. Botlhoko, T.K. Satekge, M.J. Hato, Comparative extraction and characterisation of cellulose nanostructures from sawdust and maize stalk biomass, Int. J. Biol. Macromol. 329 (2025) 147842, https://doi.org/10.1016/j.ijbiomac.2025.147842.
[14] M.J. Taherzadeh, K. Karimi, Pretreatment of lignocellulosic wastes to improve ethanol and biogas production: a review, Int. J. Mol. Sci. 9 (2008) 1621–1651, https://doi.org/10.3390/ijms9091621.
[15] L.M.R. Fuentes, L.M.M. Bastidas, O.J.M. Vargas, Selective extraction and modification of cellulose from sugar cane bagasse (Saccharum officinarum), Univ. Sci. 27 (2022), https://doi.org/10.11144/Javeriana.SC273.seam (254–272–254–272).
[16] A. Jahani, M.H. Jazayeri, Tailoring cellulose: from extraction and chemical modification to advanced industrial applications, Int. J. Biol. Macromol. 309 (2025) 142950, https://doi.org/10.1016/j.ijbiomac.2025.142950.
[17] R.S. Abolore, S. Jaiswal, A.K. Jaiswal, Green and sustainable pretreatment methods for cellulose extraction from lignocellulosic biomass and its applications: a review, Carbohydr. Polym. Technol. Appl. 7 (2024) 100396, https://doi.org/10.1016/j.carpta.2023.100396.
[18] Y. Tang, X. Shen, J. Zhang, D. Guo, F. Kong, N. Zhang, Extraction of cellulose nanocrystals from old corrugated container fiber using phosphoric acid and enzymatic hydrolysis followed by sonication, Carbohydr. Polym. 125 (2015) 360–366, https://doi.org/10.1016/j.carbpol.2015.02.063.
[19] R. Freixo, F. Casanova, A.B. Ribeiro, C.F. Pereira, E.M. Costa, M.E. Pintado, Ó. L. Ramos, Extraction methods and characterization of cellulose fractions from a sugarcane by-product for potential industry applications, Ind. Crop. Prod. 197 (2023) 116615, https://doi.org/10.1016/j.indcrop.2023.116615.
[20] M. Rizwan, S.R. Gilani, A.I. Durrani, S. Naseem, Cellulose extraction of Alstonia scholaris: a comparative study on efficiency of different bleaching reagents for its isolation and characterization, Int. J. Biol. Macromol. 191 (2021) 964–972, https://doi.org/10.1016/j.ijbiomac.2021.09.155.
[21] T. Wang, Y. Zhao, Optimization of bleaching process for cellulose extraction from apple and kale pomace and evaluation of their potentials as film forming materials, Carbohydr. Polym. 253 (2021) 117225, https://doi.org/10.1016/j.carbpol.2020.117225.
[22] A. Vazquez, M.L. Foresti, J.I. Moran, V.P. Cyras, Extraction and production of cellulose nanofibers, in: Handbook of Polymer Nanocomposites. Processing, Performance and Application: Volume C: Polymer Nanocomposites of Cellulose Nanoparticles, 2015, pp. 81–118, https://doi.org/10.1016/j.compositesb.2018.08.048.
[23] E.C. Emenike, K.O. Iwuozor, O.D. Saliu, J. Ramontja, A.G. Adeniyi, Advances in the extraction, classification, modification, emerging and advanced applications of crystalline cellulose: a review, Carbohydr. Polym. Technol. Appl. 6 (2023) 100337, https://doi.org/10.1016/j.carpta.2023.100337.
[24] D.J. McClements, Food Emulsions: Principles, Practices, and Techniques, CRC press, 2004.
[25] A. Ribeiro, J.C.B. Lopes, M.M. Dias, M.F. Barreiro, Pickering emulsions based in inorganic solid particles: from product development to food applications, Molecules 28 (2023) 2504, https://doi.org/10.3390/molecules28062504.
[26] G. Li, J. Chen, F. Zhu, Comparative study of rheological properties and Pickering emulsion stabilizing capacity of nonenyl succinic anhydride and octenyl succinic anhydride modified amaranth starches, Int. J. Biol. Macromol. 253 (2023) 126606, https://doi.org/10.1016/j.ijbiomac.2023.126606.
[27] A. Muiz, I. Klojdová, C. Stathopoulos, Utilization of by-products for preparation of Pickering particles, Eur. Food Res. Technol. 249 (2023) 3069–3083, https://doi.org/10.1007/s00217-023-04349-z.
[28] J. Lains, M.M. Dias, R. Santos, A. Ribeiro, I. Martins, Sustainable stabilisation of microcrystalline cellulose oil-in-water Pickering emulsions, Colloids Surf. A Physicochem. Eng. Asp. 727 (2025) 138419, https://doi.org/10.1016/j.colsurfa.2025.138419.
[29] H. Chen, Q. Wang, Z. Rao, X. Lei, J. Zhao, L. Lei, J. Ming, The linear/nonlinear rheological behaviors of Pickering emulsion stabilized by Zein and Xanthan gum: effect of interfacial assembly strategies, Food Hydrocoll. 145 (2023) 109116, https://doi.org/10.1016/j.foodhyd.2023.109116.

[30] A.C. Csakvari, A. Lupitu, S. Bungău, M.A. Gitea, D. Gitea, D.M. Ţiţ, L. Copolovici, S. Nemeth, D. Copolovici, Fatty acids profile and antioxidant activity of almond oils obtained from six Romanian varieties, Farmacia 67 (2019) 882–887, https://doi.org/10.31925/farmacia.2019.5.19.
[31] J.T. Oberlerchner, T. Rosenau, A. Potthast, Overview of methods for the direct molar mass determination of cellulose, Molecules 20 (2015) 10313–10341, https://doi.org/10.3390/molecules200610313.
[32] M.R. Kasaai, Comparison of various solvents for determination of intrinsic viscosity and viscometric constants for cellulose, J. Appl. Polym. Sci. 86 (2002) 2189–2193, https://doi.org/10.1002/app.11164.
[33] A. Ribeiro, Y.A. Manrique, J.C.B. Lopes, M.M. Dias, M.F. Barreiro, Development of water-in-oil Pickering emulsions from sodium oleate surface-modified nano-hydroxyapatite, Surf. Interfaces 29 (2022) 101759, https://doi.org/10.1016/j.surfin.2022.101759.
[34] S. Zhang, Y. Mei, G. Lin, Pyrolysis interaction of cellulose, hemicellulose and lignin studied by TG-DSC-MS, J. Energy Inst. 112 (2024) 101479, https://doi.org/10.1016/j.joei.2023.101479.
[35] M. Poletto, Assessment of the thermal behavior of lignins from softwood and hardwood species, Maderas. Ciencia y Tecnología 19 (2017) 63–74, https://doi.org/10.4067/S0718-221X2017005000006.
[36] X. Zhang, C. Fang, Y. Cheng, M. Li, J. Liu, Fine extraction of cellulose from corn straw and the application for eco-friendly packaging films enhanced with polyvinyl alcohol, Int. J. Biol. Macromol. 268 (2024) 131984, https://doi.org/10.1016/j.ijbiomac.2024.131984.
[37] U. Harini, S. Harish, A. Harishankar, M. Buvaneswaran, V. Sinija, Extraction and characterization of microcrystalline cellulose from wine waste, Food Bioprod. Process. 144 (2024) 92–101, https://doi.org/10.1016/j.fbp.2024.01.001.
[38] A.G. Barneto, C. Valls, J. Ariza, M.B. Roncero, Thermogravimetry study of xylanase-and laccase/mediator-treated eucalyptus pulp fibres, Bioresour. Technol. 102 (2011) 9033–9039, https://doi.org/10.1016/j.biortech.2011.07.061.
[39] J. Fang, R. Sun, J. Tomkinson, Isolation and characterization of hemicelluloses and cellulose from rye straw by alkaline peroxide extraction, Cellulose 7 (2000) 87–107, https://doi.org/10.1023/A:1009245100275.
[40] J.A. Sirviö, A.M. Kantola, A. Ämmälä, Cellulose nanofibers from nonbleached and hydrogen peroxide bleached acidic thiourea treated sawdust, J. Clean. Prod. 423 (2023) 138824, https://doi.org/10.1016/j.jclepro.2023.138824.
[41] P. Nawangsari, W. Fatra, A. Kusuma, M. Badri, D. Masnur, Microcellulose from pineapple leaf fiber as a potential sustainable material: extraction and characterization, Jurnal Polimesin. 22 (2024), https://doi.org/10.30811/jpl.v22i1.
[42] V. Chanthavong, M. Prabhakar, D.W. Lee, J.-i. Song, Extraction of cellulose microfibers from waste fallen dried leaves and fabrication of a degradable composite film for packaging applications, J. Inorg. Organomet. Polym. Mater. 34 (2024) 1861–1875, https://doi.org/10.1007/s10904-023-02928-x.
[43] A. Ribeiro, Y.A. Manrique, I.C. Ferreira, M.F. Barreiro, J.C.B. Lopes, M.M. Dias, Nanohydroxyapatite (n-HAp) as a Pickering stabilizer in oil-in-water (O/W) emulsions: a stability study, J. Dispers. Sci. Technol. 43 (2022) 814–826, https://doi.org/10.1080/01932691.2020.1845199.
[44] R. Gómez-García, S.C. Sousa, Ó.L. Ramos, D.A. Campos, C.N. Aguilar, A. R. Madureira, M. Pintado, Obtention and characterization of microcrystalline cellulose from industrial melon residues following a biorefinery approach, Molecules 29 (2024) 3285, https://doi.org/10.3390/molecules29143285.
[45] B. Hariyanto, D. Wardani, N. Kurniawati, N. Har, N. Darmawan, I. Husein, X-ray peak profile analysis of silica by Williamson–Hall and size-strain plot methods, J. Phys. Conf. Ser. 2021 (2019) 012106, https://doi.org/10.1088/1742-6596/2019/1/012106.
[46] I. Maj, K. Niesporek, P. Płaza, J. Maier, P. Łój, Biomass ash: a review of chemical compositions and management trends, Sustainability 17 (2025) 4925, https://doi.org/10.3390/su17114925.
[47] S. Abdulrahman, K. Al-Kaream, E. Azal, Enhancing soil with low-cost Pozzolanic materials: rice husk ash and groundnut shell ash compared to cement, Math. Model. Eng. Probl. 11 (2024), https://doi.org/10.18280/mmep.110430.
[48] R.D. Kale, P.S. Bansal, V.G. Gorade, Extraction of microcrystalline cellulose from cotton sliver and its comparison with commercial microcrystalline cellulose, J. Polym. Environ. 26 (2018) 355–364, https://doi.org/10.1007/s10924-017-0936-2.
[49] S. Haward, V. Sharma, C. Butts, G. McKinley, S. Rahatekar, Shear and extensional rheology of cellulose/ionic liquid solutions, Biomacromolecules 13 (5) (2012) 1688–1699, https://doi.org/10.1021/bm300407q.
[50] N. Utomo, B. Nazari, D. Parisi, R. Colby, Determination of intrinsic viscosity of native cellulose solutions in ionic liquids, J. Rheol. 64 (2020) 1063–1073, https://doi.org/10.1122/8.0000015.
[51] K. Ahn, S. Zaccaron, T. Rosenau, A. Potthast, How alkaline solvents in viscosity measurements affect data for oxidatively damaged celluloses. Cupri-ethylenediamine (CED, cuen), Biomacromolecules (2019), https://doi.org/10.1021/acs.biomac.9b00956.
[52] A.F. Lehrhofer, M. Bacher, I. Melikhov, I. Sulaeva, W. Lindner, M. Kohout, H. Kamitakahara, A. Potthast, T. Rosenau, H. Hettegger, Elution revolution: reversing chiral recognition by swapping d- for l-cellulose, Carbohydr. Polym. 367 (2025) 123896, https://doi.org/10.1016/j.carbpol.2025.123896.
[53] K. Chitbanyong, G. Hou, P.T. Arnandan, R. Hou, I. Shibata, A. Isogai, Chemical structures and molar masses of water-soluble TEMPO-oxidized products prepared from 20% NaOH-treated cellulose, Carbohydr. Polym. 368 (2025) 124142, https://doi.org/10.1016/j.carbpol.2025.124142.
[54] J. Liu, S. Lv, Y. Mu, J. Tong, L. Liu, T. He, Q. Zeng, D. Wei, Applied research and recent advances in the development of flexible sensing hydrogels from cellulose: a review, Int. J. Biol. Macromol. (2024) 136100, https://doi.org/10.1016/j.ijbiomac.2024.136100.
[55] G. Hou, K. Chitbanyong, I. Shibata, A. Isogai, Can high-molar-mass cellulose molecules be extracted from phosphorylated pulp and TEMPO-oxidized pulps or their nanofibrils using LiCl/DMAc? Carbohydr. Polym. 367 (2025) 124035 https://doi.org/10.1016/j.carbpol.2025.124035.
[56] X. Li, J. Li, Y. Kuang, S. Guo, L. Mo, Y. Ni, Stabilization of Pickering emulsions with cellulose nanofibers derived from oil palm fruit bunch, Cellulose 27 (2020) 839–851, https://doi.org/10.1007/s10570-019-02803-4.
[57] Z. Li, H. Wu, M. Yang, D. Xu, J. Chen, H. Feng, Y. Lu, L. Zhang, Y. Yu, W. Kang, Stability mechanism of O/W Pickering emulsions stabilized with regenerated cellulose, Carbohydr. Polym. 181 (2018) 224–233, https://doi.org/10.1016/j.carbpol.2017.10.080.
[58] L. Bai, S. Lv, W. Xiang, S. Huan, D.J. McClements, O.J. Rojas, Oil-in-water Pickering emulsions via microfluidization with cellulose nanocrystals: 1. Formation and stability, Food Hydrocoll. 96 (2019) 699–708, https://doi.org/10.1016/j.foodhyd.2019.04.038.
[59] J.-r. Qi, L.-w. Song, W.-q. Zeng, J.-s. Liao, Citrus fiber for the stabilization of O/W emulsion through combination of Pickering effect and fiber-based network, Food Chem. 343 (2021) 128523, https://doi.org/10.1016/j.foodchem.2020.128523.
[60] J. Buffiere, Z. Balogh-Michels, M. Borrega, T. Geiger, T. Zimmermann, H. Sixta, The chemical-free production of nanocelluloses from microcrystalline cellulose and their use as Pickering emulsion stabilizer, Carbohydr. Polym. 178 (2017) 48–56, https://doi.org/10.1016/j.carbpol.2017.09.028.
[61] A.A.D. Meirelles, A.L.R. Costa, R.L. Cunha, The stabilizing effect of cellulose crystals in O/W emulsions obtained by ultrasound process, Food Res. Int. 128 (2020) 108746, https://doi.org/10.1016/j.foodres.2019.108746.